Bistability with Optical Beams Propagating in a Reorientational Medium

Nina Kravets,[1] Armando Piccardi,[1] Alessandro Alberucci,[1] Oleksandr Buchnev,[2] Malgosia Kaczmarek,[2] and Gaetano Assanto[1,*]
[1]NooEL–Nonlinear Optics and OptoElectronics Lab, University "Roma Tre", 00146 Rome, Italy
[2]Zepler Institute, University of Southampton, Southampton SO17 1BJ, United Kingdom
(Received 17 February 2014; published 7 July 2014)

We investigated bistability with light beams in reorientational nematic liquid crystals. For a range of input powers, beams can propagate as either diffracting or self-trapped, the latter corresponding to spatial solitons. The first-order transition in samples exhibiting abrupt self-focusing with a threshold is in agreement with a simple model.

DOI: 10.1103/PhysRevLett.113.023901 PACS numbers: 42.65.Pc, 05.45.Yv, 42.65.Tg, 78.15.+e

Bistability is a fascinating phenomenon in physics and optics. It also plays a pivotal role in electronics, as systems with internal states that depend on their past evolution are the basis of memories and latch elements. In optics, several approaches have been undertaken to achieve optical bistability, i.e., the copresence of two stable states for a given excitation, in which two main ingredients, nonlinear response and feedback [1], were exploited. These approaches include cavities with saturable absorbers [2] or materials with an intensity-dependent refractive index [3], distributed feedback structures [4,5], self-focusing and reflection in Kerr-like media [6,7], increasing absorption versus power [8], linear or nonlinear interfaces [9], and distributed coupling to nonlocal waveguides [10]. Optical bistability was also investigated in plasmonic nanostructures [11], disordered cavities [12], and photonic crystals [13], leading to all-optical memories in InP [14] and Si-compatible devices [15]. Hysteresis was recently reported in QED cavities [16]. Bistable solitons were predicted in media with a nonlinear dependence of the refractive index on light intensity [17,18], but were never observed.

In this Letter, at variance with previous theoretical predictions on bistable solitons [17,18], we discuss and demonstrate bistability with optical beams propagating in reorientational nonlinear media, nematic liquid crystals (NLCs), as either diffracting or self-confined wave packets. Most NLCs are positive uniaxial fluids with long-range orientational order and optic axis set by the alignment of the elongated molecules, as described by the director $\hat{n}(x, y, z)$ [19,20]. The two extremal values of the refractive index are $n_{\parallel}$ and $n_{\perp}$ for electric fields along and normal to $\hat{n}$, respectively. Spatial optical solitons in NLCs (or "nematicons" [21]) have been widely investigated because of potential applications and unique medium characteristics, including high nonlocality and nonlinearity, high damage threshold and extended spectral transparency, and external tunability of both linear and nonlinear dielectric properties [19,20]. The physics of nonlinear reorientation is relatively straightforward: The extraordinarily polarized electric field of the beam induces dipoles in the anisotropic NLC molecules, which undergo a torque and rotate towards the field vector to minimize the overall energy; the resulting orientation is then determined by the balance between torque and intermolecular interactions. Because of the rotation of the optic axis, the extraordinary refractive index increases with optical excitation, and its distribution forms a waveguide for light itself [21].

The reorientational response differs from the standard Kerr type. Its highly nonlocal character supports stable solitons even in $(2+1)$D geometries [22]. The light-driven refractive index change depends on the sine of the angle between electric field $\mathbf{E}$ and director $\hat{n}$ [20], so that the nonlinear strength can be adjusted with the initial director alignment [23,24]. When the vectors $\mathbf{E}$ and $\hat{n}$ are initially orthogonal (see Fig. 1), reorientation can only take place

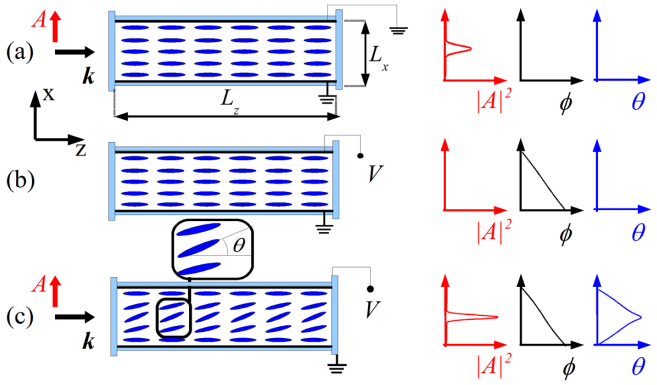

FIG. 1 (color online). Left: Side view of a NLC planar glass cell with thin film electrodes for voltage bias and director $\hat{n}$ anchored parallel to $\hat{z}$ at the boundaries. $\boldsymbol{A}$ and $\boldsymbol{k}$ indicate the beam electric field vector and wave vector, respectively. Right: Sketches of electric potential ϕ, beam intensity at the cell output $[|A|^2(z = L_z)]$, and director orientation θ versus NLC thickness x. (a) In an unbiased cell, no reorientation occurs for input powers below OFT. (b) Without light and for bias below the (electric) Fréedericksz threshold, θ remains zero. (c) The simultaneous presence of a light beam and voltage allows for the overcoming of the Fréedericksz transition; the director reorients in the bulk.

beyond a threshold associated with the optical Fréedericksz transition (OFT) [25] (the electric Fréedericksz transition is driven by voltage). While OFT usually is a second-order transition [19], specific configurations were studied to obtain first-order transitions and hysteresis [7,26–35].

Geometries exhibiting a threshold have a steplike nonlinear response and should support soliton bistability [17]; hence, reorientational NLCs subject to OFT can be expected to exhibit bistability between states corresponding to self-trapped (solitary) and diffracting (linear) beams. Intuitively, for a finite beam (e.g., Gaussian), the threshold power depends on the waist [see Fig. 2(a)] and diffraction. When the input power is increased, once the OFT threshold is overcome and reorientation occurs, self-focusing reduces the beam size and generates a self-confined wave packet; from the latter state, when the power is decreased, the dynamics of the narrower solitary beam no longer obeys the previous reorientational curve. The OFT threshold (from nonlinear to linear regimes) becomes lower, and thus leads to bistability (and hysteresis) between the two threshold values. Analogous to mirrorless optical bistability [6,8], the first-order transition stems from light self-action: Above the threshold, the beam changes the refractive index, yielding self-focusing and modifying its intensity distribution (hence the threshold). In turn, the latter determines the beam whereabouts as the input power decreases back to low (linear) values.

In this Letter, we refer to a planar NLC cell as in Fig. 1, which contains the standard mixture E7. The rubbing of the confining glass slides ensures strong anchoring (planar on top and bottom interfaces and homeotropic on input and output facets) [19], so the director is uniformly parallel to $\hat{z}$; i.e., $\theta = 0$ everywhere at rest, with θ the angle of $\hat{n}$ with the propagation axis z. The NLC sample has a thickness $L_x = 100\ \mu$m along x and extends for $L_z = 1.5$ mm longitudinally; it can be assumed to be infinitely wide versus y. Thin films of indium tin oxide deposited on the inner interfaces permit the application of a low-frequency voltage V across L_x, with a nearly uniform electric field $E_{\rm LF} \approx V/L_x$. Because reorientation is nonresonant, both low- and optical-frequency fields can contribute to changing the director distribution.

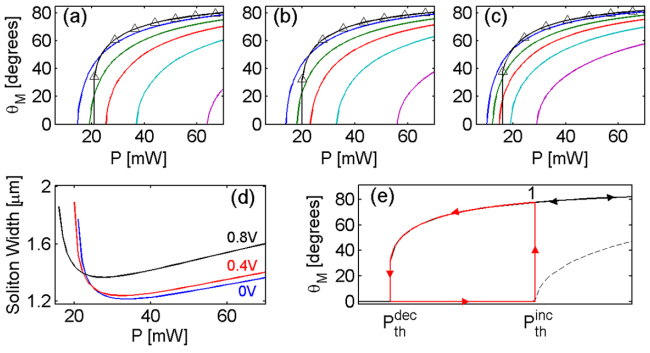

FIG. 2 (color online). Maximum reorientation θ_M versus power for V equal to (a) 0.0, (b) 0.4, and (c) 0.8 V, respectively. Solid lines in color correspond to $w_{\rm in} = 2$, 5, 10, 20, and 40 μm from left to right (blue to magenta), whereas black lines with triangles show θ_M once a soliton is formed. (d) Soliton size versus power. (e) Sketch of hysteresis for $w_{\rm in} = 40\ \mu$m and $V = 0.4$ V; the dashed line refers to reorientation without self-focusing. Here $K = 12 \times 10^{-12}$ N (as in E7), $\lambda = 1064$ nm, and $L_x = 100\ \mu$m.

The optical excitation (at $\lambda = 1.064\ \mu$m) is a continuous-wave single-humped (fundamental Gaussian) beam polarized along x, launched in $z = x = 0$ with wave vector $\boldsymbol{k} \| \hat{z}$. The beam electric field is $Ae^{ik_0 n_\perp z}$ ($k_0 = 2\pi/\lambda$, the vacuum wave number), with A the slowly varying envelope. We assume all of the elastic constants to be K [19,20], and we define the optical and low-frequency dielectric anisotropies $\epsilon_a = \epsilon_\parallel - \epsilon_\perp = n_\parallel^2 - n_\perp^2$ and $\Delta\epsilon_{\rm LF}$, respectively [19]. Neglecting birefringent walk-off, the time-independent evolution of an extraordinary polarized beam is described by

$$2ik_0 n_\perp \frac{\partial A}{\partial z} + D_x \frac{\partial^2 A}{\partial x^2} + \frac{\partial^2 A}{\partial y^2} + k_0^2 \Delta n_e^2(\theta) A = 0, \quad (1)$$

$$\nabla^2 \theta + \frac{\epsilon_0}{2K}\left(\frac{\epsilon_a |A|^2}{2} + \Delta\epsilon_{\rm LF} E_{\rm LF}^2\right) \sin(2\theta) = 0, \quad (2)$$

with $D_x = n_e^2(\theta)/\epsilon_{zz}$ as the diffraction coefficient in xz [$\epsilon_{jk}(\theta) = \epsilon_\perp \delta_{jk} + \epsilon_a n_j n_k$ ($j,k = x,y,z$), with $n_{j/k}$ the Cartesian components of $\hat{n}$] [36]. The photonic potential $\Delta n_e^2(\theta) = n_e^2(\theta) - n_\perp^2$ depends on both bias V and field A according to Eq. (2), thus accounting for nonlinearity [23]. Equation (1) governs light propagation in NLCs, according to the potential Δn_e^2; the distribution of n_e is determined by the balance between the external (optic and electric) torque and the restoring elastic forces [Eq. (2)]. Models similar to Eqs. (1)–(2) apply to solitons in other systems (without OFT), e.g., quadratic and thermo-optic media [37].

For a simple insight into the optics of the phenomenon, we first discuss the solution of Eq. (2) in the (propagation-invariant) limit $\partial_z = 0$, for a Gaussian profile and various input waists $w_{\rm in}$, adding a small perturbation on the initial θ to break the system symmetry. Figures 2(a)–2(c) show the maximum reorientation θ_M for three biases. As expected, molecular reorientation undergoes a second-order transition due to the size of ϵ_a [19,26]. In this geometry both light- and voltage-driven torques tend to rotate the director in the same direction; thus, the bias works against first-order optical transitions [29]. For a given voltage, the narrower the beam, the lower the OFT power threshold [20]; higher $E_{\rm LF}$ [from panels (a) to (c) in Fig. 2] reduces the threshold and the power required for each θ_M.

Next, we look for solitary waves obeying Eqs. (1)–(2) in NLCs encompassing a z-invariant director distribution; the latter assumption implies the lack of elastic forces exerted by input and output interfaces on the director (weak anchoring) and no propagation losses [24]. Substituting the soliton ansatz $A = u_s(x,y)e^{ik_0 n_s z}$ and $\theta = \theta_s(x,y)$ leads to a nonlinear eigenvalue problem; its solutions are plotted in

Fig. 2(d) and as black lines with triangles in Figs. 2(a)–2(c) (see Supplemental Material, Section 1 [38]). Owing to OFT, solitons never exist at powers below $P_{\rm th}^{\rm dec}$, and $P_{\rm th}^{\rm dec}$ decreases as the applied voltage increases [various lines in Fig. 2(d)]. Assuming an initial Gaussian intensity profile of waist $w_{\rm in}$, a nematicon forms only above $P_{\rm th}^{\rm inc}$, the latter depending on $w_{\rm in}$, consistently with the reorientation trend for a given beam profile. Conversely, once reorientation has occurred, the self-confined beam no longer depends on $w_{\rm in}$, i.e., the memory of the previous (linear) state is lost.

To illustrate optical bistability, let us simply consider a beam of waist $w_{\rm in}$ launched in the cell, with $w_{\rm in}$ and V chosen to yield OFT at powers $> P_{\rm th}^{\rm dec}$. Until the power reaches $P_{\rm th}^{\rm inc}$ [lower branch in Fig. 2(e)], θ_M remains zero, as nonlinear effects do not take place. Above $P_{\rm th}^{\rm inc}$ the director rotates and a nematicon forms [point 1 in Fig. 2(e)], with θ_M following the reorientation curve in the presence of self-trapping. The beam size is now set by the soliton existence curve in Fig. 2(d). When the power decreases [from point 1, upper branch in Fig. 2(e)], this narrower (solitary) beam evolves along the black line with triangles in Figs. 2(a)–2(c), experiencing a lower power threshold $P_{\rm th}^{\rm dec}$, independently from $w_{\rm in}$. Between $P_{\rm th}^{\rm dec}$ and $P_{\rm th}^{\rm inc}(w_{\rm in})$, two stable states exist, owing to the light's ability to modify the index distribution n_e. In this model, bistability does not occur for small waists, and wider hysteresis cycles correspond to larger $w_{\rm in}$; moreover, such bistable behavior is not restricted to NLCs with specific anisotropy or elastic response [26,29].

In experiments, the propagation dynamics cannot be ignored, as losses and longitudinal nonlocal effects are present, as, e.g., in nonlinear distributed couplers [39,40]. Below OFT, the (linear) beam profile changes with z, making the threshold power depend on the diffractive properties, such as Rayleigh length and waist location. Even after the nematicon is generated, the sample is not z invariant, due to boundary conditions $\theta = 0$ on the input and output facets. Finally, nematicons change width and power because of both unavoidable scattering and their breathing character [21,41]. In short, the inherent beam dynamics, even in the solitary regime, is expected to produce quantitative discrepancies between the experimental results and the theoretical predictions of Fig. 2.

We carried out the experiments by varying the input beam power stepwise and ensuring that the system reached a steady state (e.g., waiting from tens of seconds up to several minutes near the transitions) before each measurement. In unbiased cells [i.e., $E_{\rm LF} = 0$ V/m in Eq. (2)], OFT could only be achieved at powers high enough (≈50 mW) to cause temporal instabilities [42] (see Supplemental Material, Section 2 [38]); hence, we biased the sample across x to lower the threshold. Our calculations indicated that a bias of $V = 0.92$ V, which is below the electric Fréedericksz threshold, could considerably reduce the OFT threshold (see trend in Fig. 2) and help the observation of bistability. The calculations also showed that the hysteresis cycle could be widened at lower temperatures (Supplemental Material, Section 3 [38]), e.g., by cooling the sample with a Peltier cell. The experimental results confirmed that a voltage $V = 0.92$ V was low enough to not induce reorientation without light (see Supplemental Material, Section 4 [38]), but was adequate to minimize the input power required for OFT. In a sample at 18 °C, a Gaussian beam of waist $w_{\rm in} \approx 2$ μm diffracted at low powers, whereas from 16 to about 20 mW it overcame OFT, self-focused (without spurious effects), and formed a nematicon.

Figure 3 displays the beam evolution in the yz plane when power was first ramped up from 1 to 20 mW, and then down from 20 to 1 mW; (b,c) illustrate the beam evolution in the lower branch of the hysteresis while (b*,c*) that in the upper branch. Figure 4 graphs the acquired beam size ($w = 2\sqrt{\int y^2|A|^2dy / \int |A|^2dy}$) versus z, normalized to the measured initial w_0 for various powers around the cycle. In Fig. 3(a), $P = 1$ mW corresponds to the linear diffraction, i.e., the initial and final states of the bistable cycle that is sought (below $P_{\rm th}^{\rm dec}$). For $P \approx 15$ mW [Figs. 3(b)–3(c)], higher than the power necessary to excite nematicons in threshold-free geometries [21], modest self-focusing occurred with the beam size monotonically increasing along z due to the prevailing diffraction [green line with empty circle and red line with diamond in Fig. 4(a)]. For $P = 20$ mW [Fig. 3(d)] a stable nematicon was excited [violet line with triangle in Figs. 4(a)–4(b)]. Then, from this (20 mW) self-confined state, the input power was

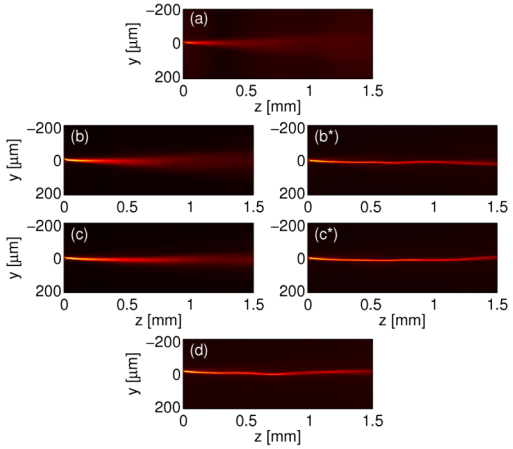

FIG. 3 (color online). Acquired images of a $w_{\rm in} \approx 2$ μm beam evolving in the plane yz for $V = 0.92$ V as power is ramped up and down. (a) Initial as well as final state without self-trapping ($P = 1$ mW); (d) soliton-state at the maximum power ($P = 20$ mW) used in the cycle. The paired panels (b,b*) and (c,c*) show the beam evolution for inputs of 14.5 and 15.5 mW, respectively, as power is raised (diffraction, left) or reduced (self-confinement, right). The initial waist appears to be $w_0 \approx 9$ μm > $w_{\rm in}$ owing to scattering-induced image blurring [41].

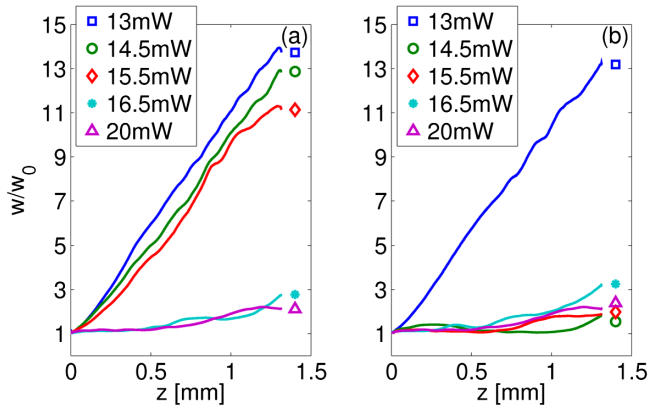

FIG. 4 (color online). Experimental results: normalized beam size w/w_0 (measured across y) versus z as the input power is ramped (a) up and (b) down from 13 to 20 mW and vice versa, respectively. Input powers are specified in the legends.

progressively reduced to the initial value of 1 mW. Figures 3(b*)–3(c*) and Fig. 4(b) (green line with empty circle and red line with diamond) show that beams propagated self-localized even at those powers for which diffraction was observed during ramp-up [Figs. 3(b)–3(c) and Fig. 4(a)]. The beam evolution exhibited "memory" of the previously determined director distribution, making the system bistable through self-action of the wave packet.

Figure 5 plots the beam mean size $\bar{w} = (1/L_z)\int_0^{L_z} w dz$ (measured from scattered light and averaged over L_z to reduce spurious effects due to longitudinal dynamics) normalized to the initial (measured) waist w_0 versus input power for both increasing (black squares) and decreasing (red circles) excitations. OFT prevents the formation of a soliton up to $P_{\rm th}^{\rm inc} = 16.5$ mW, with a beam much wider than the input. For $P > P_{\rm th}^{\rm inc}$ the beam self-confines,

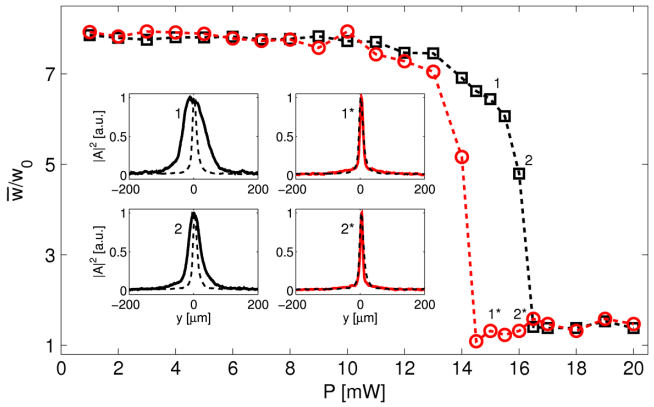

FIG. 5 (color online). Beam size $\bar{w}$ measured versus input power, averaged over L_z and normalized to the initial waist w_0. Black dashed line with squares and red dashed line with circles correspond to raising and falling powers, respectively. Insets: intensity profiles (solid lines) acquired at the cell output and compared with the measured input (dashed lines). The numerical labels refer to the corresponding points in the main plot $\bar{w}/w_0$.

with an average size comparable to w_0. When power is ramped down, self-localization is sustained as long as $P \geq P_{\rm th}^{\rm dec} = 14.5$ mW. For $P < P_{\rm th}^{\rm dec}$, the intermolecular forces restore the homogeneous distribution of θ and the linear propagation regime.

Optical bistability was observed between diffracting and self-trapping beam states in the range $P_{\rm th}^{\rm dec} < P < P_{\rm th}^{\rm inc}$. To compare experimental data and the 2D model, we calculated the director reorientation in the limit $\partial_z\theta = 0$ (as in Fig. 2), using the full tensor for the elastic constants and correcting for the actual temperature dependence (Supplemental Material, Section 3 [38]). The results, graphed in Fig. 6, show that the OFT threshold, computed for a diffracting beam with $w_{in} = 2$ μm, was comparable with that of a shape- and size-preserving Gaussian of waist ≈ 11 μm (see Supplemental Material, Section 5 [38]), with a predicted $P_{\rm th}^{\rm inc} = 5.2$ mW, nearly three times lower than measured. Such a nonunitary scaling factor between theory and experiments is expected and accounts for losses, longitudinal effects, and boundary conditions resulting in a lack of beam invariance. Applying such scaling (assumed waist independent) to the measured $P_{\rm th}^{\rm dec}$, we obtained $P_{\rm th}^{\rm dec} = 4.5$ mW, which, through the soliton reorientation curve, corresponds to a self-trapped beam of waist ≈ 3.5 μm. The latter value compares well with the observed soliton size, further confirming that system bistability stems from distinct beam widths upon self-action.

In conclusion, we investigated bistability with finite-size light beams in reorientational nematic liquid crystals encompassing self-focusing with a threshold. We observed optical bistability encompassing diffracting and self-trapped states, stemming from beam self-action in the medium. The good agreement between theoretical predictions and experiments confirms the origin of the phenomenon. These findings are expected to introduce significant novelties in optical memories as well as on latch-type switches and all-optical routers. The propagation of wave packets with multiple states in thresholded nonlinear

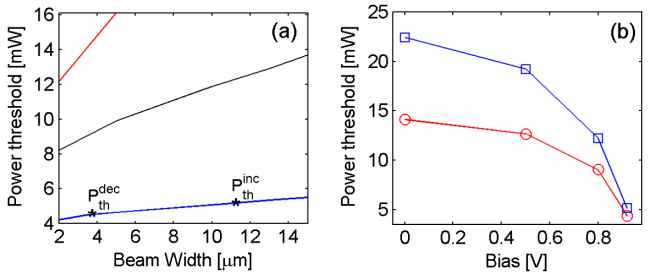

FIG. 6 (color online). (a) Calculated power threshold versus w for $V = 0$ (upper red line), $V = 0.8$ (black middle line), and $V = 0.92$ V (lower blue line); stars indicate the extrema of the observed bistable loop. (b) OFT power threshold versus bias V for $w = 3.5$ μm (nematicon size found from fitting, red line with circles) and $w = 11$ μm (linear diffracting beam, blue line with squares).

systems without external feedback, however, is a general result expected to have a radical impact on nonlinear wave dynamics in various branches of physics.

We thank Professor M. Karpierz and Professor A. A. Minzoni for helpful discussions.

*assanto@uniroma3.it; http://optow.ele.uniroma3.it

[1] H. Gibbs, *Optical Bistability: Controlling Light With Light* (Academic Press, San Diego, 1985).
[2] A. Szoke, V. Daneu, J. Goldhar, and N. A. Kurnit, Appl. Phys. Lett. **15**, 376 (1969).
[3] F. S. Felber and J. H. Marburger, Appl. Phys. Lett. **28**, 731 (1976).
[4] H. G. Winful, J. H. Marburger, and E. Garmire, Appl. Phys. Lett. **35**, 379 (1979).
[5] G. Assanto and G. I. Stegeman, Appl. Phys. Lett. **56**, 2285 (1990).
[6] J. E. Bjorkholm, A. E. Kaplan, P. W. Smith, and W. J. Tomlinson, Opt. Lett. **6**, 345 (1981).
[7] I. C. Khoo, Appl. Phys. Lett. **41**, 909 (1982).
[8] D. A. B. Miller, A. C. Gossard, and W. Wiegmann, Opt. Lett. **9**, 162 (1984).
[9] P. W. Smith, J.-P. Hermann, W. J. Tomlinson, and P. J. Maloney, Appl. Phys. Lett. **35**, 846 (1979).
[10] G. Assanto, B. Svensson, D. Kuchibhatla, U. J. Gibson, C. T. Seaton, and G. I. Stegeman, Opt. Lett. **11**, 644 (1986).
[11] G. A. Wurtz, R. Pollard, and A. V. Zayats, Phys. Rev. Lett. **97**, 057402 (2006).
[12] I. V. Shadrivov, K. Y. Bliokh, Y. P. Bliokh, V. Freilikher, and Y. S. Kivshar, Phys. Rev. Lett. **104**, 123902 (2010).
[13] M. Soljačić, M. Ibanescu, S. G. Johnson, Y. Fink, and J. D. Joannopoulos, Phys. Rev. E **66**, 055601 (2002).
[14] K. Nozaki, A. Shinya, S. Matsuo, Y. S. T. Segawa, T. Sato, Y. Kawaguchi, R. Takahashi, and M. Notomi, Nat. Photonics **6**, 248 (2012).
[15] L. Liu, R. Kumar, K. Huybrechts, T. Spuesens, G. Roelkens, E.-J. Geluk, T. de Vries, P. Regreny, D. V. Thourhout, R. Baets *et al.*, Nat. Photonics **4**, 182 (2010).
[16] Y.-D. Kwon, M. A. Armen, and H. Mabuchi, Phys. Rev. Lett. **111**, 203002 (2013).
[17] A. E. Kaplan, Phys. Rev. Lett. **55**, 1291 (1985).
[18] M. Matuszewski, W. Krolikowski, and Y. S. Kivshar, Opt. Express **16**, 1371 (2008).
[19] P. G. DeGennes and J. Prost, *The Physics of Liquid Crystals* (Oxford Science, New York, 1993).
[20] I. C. Khoo, *Liquid Crystals: Physical Properties and Nonlinear Optical Phenomena* (Wiley, New York, 1995).
[21] M. Peccianti and G. Assanto, Phys. Rep. **516**, 147 (2012).
[22] A. Snyder and D. Mitchell, Science **276**, 1538 (1997).
[23] A. Alberucci, A. Piccardi, M. Peccianti, M. Kaczmarek, and G. Assanto, Phys. Rev. A **82**, 023806 (2010).
[24] A. Alberucci and G. Assanto, Opt. Lett. **35**, 2520 (2010).
[25] S. D. Durbin, S. M. Arakelian, and Y. R. Shen, Phys. Rev. Lett. **47**, 1411 (1981).
[26] H. L. Ong, Phys. Rev. A **28**, 2393 (1983).
[27] P. Wang, H. Zhang, and J. Dai, Opt. Lett. **12**, 654 (1987).
[28] A. J. Karn, S. M. Arakelian, Y. R. Shen, and H. L. Ong, Phys. Rev. Lett. **57**, 448 (1986).
[29] S.-H. Chen and J. J. Wu, Appl. Phys. Lett. **52**, 1998 (1988).
[30] E. Santamato, G. Abbate, R. Calaselice, P. Maddalena, and A. Sasso, Phys. Rev. A **37**, 1375 (1988).
[31] E. Santamato, G. Abbate, P. Maddalena, L. Marrucci, and Y. R. Shen, Phys. Rev. Lett. **64**, 1377 (1990).
[32] M. A. Karpierz, *Soliton-Driven Photonics* (Springer, New York, 2001).
[33] E. A. Babayan, I. A. Budagovsky, S. A. Shvetsov, M. P. Smayev, A. S. Zolot'ko, N. I. Boiko, and M. I. Barnik, Phys. Rev. E **82**, 061705 (2010).
[34] I. A. Budagovsky, D. S. Pavlov, S. A. Shvetsov, M. P. Smayev, A. S. Zolot'ko, N. I. Boiko, and M. I. Barnik, Appl. Phys. Lett. **101**, 021112 (2012).
[35] F. Simoni, D. E. Lucchetta, L. Lucchetti, H. L. Ong, S. V. Serak, and N. Tabiryan, Opt. Lett. **38**, 878 (2013).
[36] A. Piccardi, M. Trotta, M. Kwasny, A. Alberucci, R. Asquini, M. Karpierz, A. d'Alessandro, and G. Assanto, Appl. Phys. B **104**, 805 (2011).
[37] E. A. Kuznetsov, A. Rubenchik, and V. Zakharov, Phys. Rep. **142**, 103 (1986).
[38] See Supplemental Material at http://link.aps.org/supplemental/10.1103/PhysRevLett.113.023901 for detailed calculations and a description of the procedures.
[39] G. I. Stegeman, G. Assanto, R. Zanoni, C. T. Seaton, E. Garmire, A. A. Maradudin, R. Reinisch, and G. Vitrant, Appl. Phys. Lett. **52**, 869 (1988).
[40] G. Vitrant, R. Reinisch, J. C. Paumier, G. Assanto, and G. I. Stegeman, Opt. Lett. **14**, 898 (1989).
[41] C. Conti, M. Peccianti, and G. Assanto, Phys. Rev. Lett. **92**, 113902 (2004).
[42] E. Braun, L. P. Faucheux, and A. Libchaber, Phys. Rev. A **48**, 611 (1993).